Physics – Uspekhi **44** (6) 617 – 629 (2001)

METHODOLOGICAL NOTES PACS numbers: **42.30.–d**, **87.16.–b**, 87.64.Rr

Coherent phase microscopy of intracellular processes

V P Tychinskiĭ

DOI: 10.1070/PU2001v044n06ABEH000841

Contents

Abstract. Information encoded in DNA implicitly determines the sequence of processes at different organizational levels of living matter. Optical microscopy is a major source of knowledge about processes in living cells. Further progress in biology to a large extent depends on the perfection of microscopic methods based on the latest advances in laser and computer technologies. This review outlines modern functional imaging techniques for living cell microscopy with particular emphasis on dynamic coherent phase microscopy based on recording local fluctuations of refractive index. The measurement results produced with a laser phase microscope are reported.

1. Introduction

The self-organization and regulation of intracellular processes rank among the fundamental problems of biology [1]. In recent years, new microscopic techniques have been developed owing to recent progress in coherent optics, spectroscopy, and computer technology [2 – 4]. Concomitantly, important results have been achieved in molecular biomechanics [5 – 8]. For example, fluorescence microscopy combined with video filming have allowed the measurement of the rotational velocity of the γ-subunit of an isolated ATPhase complex [5, 6] which acts as the smallest known natural molecular motor. Both fluorescence and video microscopies were used to determine the angular position of a labelled actin filament attached to a γ-subunit. It was demonstrated in Ref. [7] that the activity of molecular motors is associated with a periodic 3 Hz-component in the motion of fluorescently labelled actin filaments.

In what follows, we review the results of a number of studies illustrating principal trends in contemporary microscopy. Methods of multiphoton fluorescence microscopy [2] are being successfully developed and arouse ever increasing interest. Spectral filtration and the high time resolution of fluorescence decay have ensured the identification of certain proteins, their spatial distribution and dynamics. Multifocal multiphoton microscopy (MMM) [2, 3] in which the specimen surface is simultaneously scanned by 30 focused beams generated by a pulsed titanium-sapphire laser have allowed the measurement time to be substantially reduced. The combination of MMM with 4π-microscopy further improved the axial resolution to 100 – 150 nm. In this method, the specimen to be examined was placed in the interference field created by counterpropagating coherent beams emerging from two symmetrically located objectives.

Point dark field microscopy (PDFM) [8] is an example of techniques for measuring dynamic intracellular processes. This method was used to study ATP-stimulated fluctuations of an erythrocyte membrane in real time. The method is based on photoelectric recording of light intensity variations in the visual field of microscope, caused by the displacement of the specimen edge relative to the optical axis of the objective.

The employment of lasers in microscopy made it possible to develop methods for the manipulation of microparticles and intracellular surgery, implement the principle of confocal microscopy, modulate spectral and temporal characteristics of fluorescence, and improve the accuracy of measurements and the operation speed of instruments [2, 3, 5, 9, 10].

Image analysis in modern microscopes is performed under computer control. Primary information encoded in an image and subjected to processing is of paramount importance. Classical optical microscopy [11 – 13] normally operates with natural specimen images in which the information is stored as a two-dimensional intensity (or brightness) distribution of radiation from an incoherent source, scattered by the object under examination. In order to enhance the contrast of such images, selective staining of organelles is often employed in combination with various optical techniques (phase and differential interference contrast microscopy) and computerized image processing procedures such as the background radiation subtraction [12, 13]. Images in which information is contained in the form of the intensity or spectral density distributions of radiation scattered by the object will be

V P Tychinskiĭ Moscow State Institute for Radio Engineering, Electronics and Automation
prosp.Vernadskogo 78, 117454 Moscow, Russian Federation
E-mail: tych@tych.pvt.msu.su

Received 8 August 2000, revised 7 December 2000
Uspekhi Fizicheskikh Nauk **171** (6) 649 – 662 (2001)
Translated by Yu V Morozov; edited by A Radzig

hereinafter referred to as *amplitude* images, to distinguish them from the so-called *functional* images. In functional microscopic images, primary information can be present as the two-dimensional distribution of a parameter which is not directly related to the specimen's topology, for instance, spectral fluorescence density [9, 14], stimulated Raman scattering spectrum [15] or excited state relaxation time. The intensity and fluctuation spectra of optical parameters of the specimen may serve as characteristic parameters to be measured with phase microscopes [16, 18]. An important distinctive feature of phase techniques consists in that the phase is 'naturally' normalized in the main interval of definition (2π) and its values can be determined with a high accuracy when coherent light sources are used.

It is reasonable that functional images carry complementary information to the classical ones and possess a number of peculiar properties. It should be emphasized in particular that phase images provide the possibility for superhigh resolution and may be used to record local dynamic processes [16 – 19].

A general remark on the analysis of dynamic processes fixed, for example, in a series of amplitude video images is opportune before proceeding farther.

It is almost impossible to obtain reproducible normalized quantitative characteristics of motion from *a series* of amplitude images because their contrast patterns, the number of distinguishable gradations of colours, spatial resolution, and other parameters depend on a variety of uncontrollable factors, such as illumination conditions, compensation for the background, spectral sensitivity of CCD camera, etc. Specifically, in the method of differential interference contrast (DIC) in images, there is a very complex relationship between the intensity (or brightness) distribution and the orientation of anisotropic elements of the object with respect to the light polarization plane.

The absence of normalized parameters independent of illumination conditions is the main obstacle precluding *quantitative* comparison of the characteristics of amplitude images obtained with the aid of different devices.

Nevertheless, limited quantitative information about the tracks of moving particles and other dynamic processes can be derived from amplitude video images using modern computer-assisted techniques. For example, the Hamamatsu Corporation has developed optoelectronic adapters, the Argus-20-100. Its CCD camera is attached to an ordinary microscope to analyze the real-time amplitude images on the screen of a computer monitor using software developed for this task. The adapter also serves to subtract frames and observe morphological changes in colorless cells with the high spatial resolution inherent in the differential contrast technique. However, this method appears to be of limited value for investigations into intracellular dynamics and in consequence reports on recording other quantitative characteristics, for instance, fluctuation spectra and correlation functions, are lacking from the scientific literature.

Confocal microscopic techniques are widely employed in current research and proved very useful for reconstructing three-dimensional images of cells and their organelles. These methods take advantage of the linear relationship between radiation intensity at a conjugate point of the image plane and the intensity of scattering by local inhomogeneity in the object plane. Companies supplying confocal microscopes point out in their catalogues the possibility, in principle, of recording intracellular dynamic processes. However, we failed to find such measurement results reported in the available scientific literature. This can probably be accounted for as follows.

In confocal microscopes, the photocurrent is proportional to the local intensity of scattered light. Hence, only optically dense elements of the object of interest can be recorded. This means that processes leading to no appreciable changes in local optical density of the unstained object can hardly be detected.

During the last decade, further progress in submicron microscopy has been thought to depend on the development of stable and reliable probes. Certain companies announced tunnel, atomic-force, and other types of microscopes with as high a resolution as is necessary for research at the atomic level. Their optical analogues are near-field microscopes. As a rule, images in such microscopes are produced by raster scanning the object surface with an optical probe and recording the scattered light intensity. Recent direct measurements of intracellular dynamics in a saline buffer [10, 11] have confirmed that probe techniques provide a promising research tool despite certain intrinsic inconveniences (the necessity to clean or replace the needle, difficulties in matching with the visual channel).

For all that, probe techniques are not to be regarded as completely noninvasive because field gradients in the vicinity of the probe, mechanical perturbations, contact with foreign material, and other factors may influence the object characteristics. Moreover, probe techniques are not free from the disadvantages inherent in amplitude images. The quantity being measured, i.e. light intensity variation at the output of the optical probe, ought to be normalized. Otherwise, it is difficult (if not impossible) to compare it with physical quantities measured by other methods and identify it with biological parameters adopted. The sensitivity, resolving power, and operation speed of probe microscopes are quite sufficient for the investigation of many intracellular processes. Few publications are however available on the subject.

Phase images feature the two-dimensional phase distribution or the optical path difference (OPD) of interfering beams. A traditional area of research using phase microscopes is profilometry of the surface microstructure and microelectronics. The geometric profile height $H(x, y)$ of optically homogeneous opaque objects is related to the phase $\varphi(x, y)$ of the reflected wave by the trivial relation

$$H(x, y) = \frac{4\pi\varphi(x, y)}{\lambda} .$$

In images of optically inhomogeneous transparent objects, the OPD is in a certain approximation proportional to the local projection of the refractive index $n(x, y)$ onto the beam direction z:

$$h(x, y) = \frac{4\pi\varphi(x, y)}{\lambda} = \int_0^{H(x,y)} n(x, y, z)\,\mathrm{d}z .$$

A phase or OPD is measured by interference microscope with the modulation of the reference wave phase [20, 21]. In multistep modifications [20] of phase microscopy, a coordinate-sensitive photodetector (usually a CCD camera) is used at a fixed reference wave phase to record and load into a computer memory a certain number of interference field intensity patterns $I_q(X, Y)$ to be able to compute the local phase value or OPD for each pixel of the image. Here, X, Y are the coordinates in the image plane, and q is the reference wave phase index.

For an interference field intensity represented in the form

$$I_q(X, Y) = a(X, Y) + b(X, Y)\cos\left[\varphi(X, Y) + \Delta\varphi_q\right],$$

and at fixed reference wave phase values

$$\Delta\varphi_q = \frac{\pi q}{2},$$

where $q = 1, 2, 3, \ldots, n$, the phase is found from the formulas

$$\varphi = \operatorname{arctg}\frac{I_4 - I_2}{I_1 - I_3}, \qquad \varphi = \operatorname{arctg}\frac{2I_4 - 2I_2}{I_1 - 2I_3 + I_5}$$

for four ($n = 4$) and five ($n = 5$) steps, respectively. Local phase values can be calculated using the above algorithms from patterns $I_q(X, Y)$, in each pixel of the image (X, Y), stored in the computer memory.

The multistep method ensures a high measurement accuracy for stationary interference fields, fast operation speed, and a large number of pixels. Major disadvantages of this technique are due to the fact that local phase values are determined from patterns $I_q(X, Y)$ measured at different time instants. For this reason, intensity and frequency fluctuations of the radiation source as well as vibrations and mechanical instability of the interferometer restrict the measurement accuracy. The same reason accounts for the impossibility of recording intracellular dynamic processes by the method in question.

A serious problem is the interpretation of information obtained with the use of microscopic techniques. This is especially true so far as functional images are concerned. Therefore, the current tendency towards the development of multifunctional microscopes [9] and extensive application of modern software for image processing appears to be fully justified.

2. Physical basis of coherent microscopy

In the following pages, we shall consider at length a method for the construction of phase images [18, 22], which enabled us to realize a solution to the problem of intracellular dynamic microscopy.

There are several inevitable, serious obstacles to the practical realization of phase microscopic techniques. Indeed, a native biological object to be examined in a thin layer *in vitro* may be regarded as a structured optically inhomogeneous anisotropic medium which is impossible to describe by a single coordinate function in the image plane.

For example, the optical density distribution or OPD in phase images is linked to the projection of the refractive index tensor $n(r, t)$, and cellular organelles can be identified based on *a priori* information (a more compact nucleus, enhanced density gradients close to cellular membranes, etc.). Biological objects for *in vitro* microscopy are normally prepared as a layer of cells or organelles suspended in a buffer solution and placed in a cuvette or mounted on a glass slide. Therefore, as an adequate physical model in the confined field of view of the lens L (see Fig. 1) may serve a layer of an immersion liquid with refractive index n_0 placed under a cover glass G and containing an optical inhomogeneity of size d, thickness H, and refractive index tensor $n(r, \omega, t)$, where n depends on ω (light source frequency). The interference field intensity and scattered wave phase $\varphi(X, Y)$ are measured with a photodetector at each point of the image plane (X, Y).

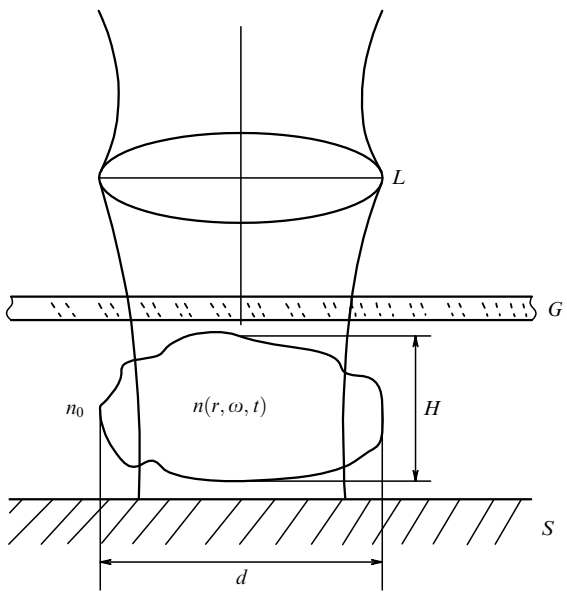

Figure 1. Model of a biological object. An optically inhomogeneous element $n(r, \omega, t) = n(r) + \delta n(r, \omega, t)$ of a transverse size d and thickness H is immersed in a liquid with the refractive index n_0 and placed on a polished substrate S under a cover glass G in the field of view of the lens L. The phase at each point of the image is proportional to the projection of the refractive index.

In the eikonal approximation [23], the scattered wave field $E(r, t)$, where $r[x, y, z]$ are the coordinates near the object plane, may be represented by local plane waves

$$E(r, t) = E_0(r)\exp\left[-jk_0S(r) + j\omega t\right],$$

where $E_0(r)$ is a slowly changing function of coordinates, $k_0 = \omega/c$, and $S(r)$ is the eikonal satisfying the condition $(\nabla S)^2 = n(r)^2$. In the geometrical optics approximation $k_0\nabla S = k(r)$ and at

$$\frac{\mathrm{d}S}{\mathrm{d}x}, \frac{\mathrm{d}S}{\mathrm{d}y} \ll \frac{\mathrm{d}S}{\mathrm{d}z}$$

the scattered wave phase is proportional to the projection of the refractive index at the point (x, y) in the object plane:

$$\varphi(x, y) = k_0S(x, y) = k_0\int n(x, y, z)\,\mathrm{d}z = k_0h(x, y).$$

The microscope optical system cuts off high spatial frequencies in the field $E(r, t)$ and transfers the object-modulated ith wave into the image plane X, Y:

$$E_\Sigma(X, Y, t) = \sum_i E_i(r, t) \otimes P(X, Y, r),$$

where $P(X, Y, r)$ is the coherent transfer function of the objective [11, 23], and $\otimes$ denotes convolution.

Modulation of the wave front $\varphi(x, y)$ in the object plane is transferred, up to high spatial frequencies, into the image plane:

$$\varphi(x, y) \cong \varphi(X, Y),$$

where $X/x = Y/y = M$ is the linear optical magnification.

Interferometers measure the phase difference

$$\Delta\varphi(X, Y, t) = \arg\left[E_\Sigma(X, Y, t)\right]$$

of the wave scattered by the object:

$$\Delta\varphi(X, Y) = \frac{2\pi h(X, Y)}{\lambda}$$

or OPD $h(X, Y)$ at different points of the wave front. The functions $\varphi(X, Y)$ and $h(X, Y)$ will be considered below as phase images of the object $n(x, y, z)$. It should be recalled that functions $\varphi(X, Y)$ are determined to within an additive constant and do not always provide an unambiguous characteristic of the object. For example, $\varphi(X, Y)$ may depend on the numerical aperture of the objective, the accuracy of focusing, and the polarization of the transmitted wave.

In the geometrical optics approximation, the local inhomogeneity $n(x, y, z)$ of large transverse size ($d \gg \lambda$) and axial height $H(x, y)$ has a phase 'portrait'

$$\Delta\varphi(X, Y) = \frac{2\pi h(X, Y)}{\lambda},$$

where the OPD

$$h(X, Y) \approx h(x, y) = \int_0^{H(x,y)} n(x, y, z)\,\mathrm{d}z \qquad (1)$$

is the 'projection' of the function $n(x, y, z)$ within the limits of integration 0 and $H(x, y)$, respectively. For an optically homogeneous object in the immersion medium n_0, one obtains

$$h(X, Y) \approx h(x, y) = H(n - n_0).$$

Mind that X, Y and x, y are the coordinates of conjugate points in the image and object planes. Naturally, it is impossible in such a 'portrait' to distinguish between the contributions coming from the height $H(x, y)$ and refractive index $n(x, y, z)$.

A similar uncertainty arises in a layered medium, when the total contribution of individual layers is measured:

$$h(r) = \sum_k n_k H_k, \quad k = 1, 2, 3, \ldots$$

It follows from Eqn (1) that phase images must show systematic differences between geometric $H(X, Y)$ and 'phasic' $h(X, Y)$ heights. The 'phasic' height $h(X, Y)$ depends on the local difference between the projections of refractive indices, for instance, in the inhomogeneity $n(r, \omega, t)$ and buffer n_0 in Fig. 1. Normally, the following inequality holds:

$$\left[n(r, \omega, t) - n_0\right] \ll 1.$$

Therefore, the *measured* phase height (OPD) is smaller than the real (geometric) thickness:

$$h(X, Y) \ll H(x, y).$$

The interpretation of phase 'portraits'

$$\Delta\varphi(X, Y) = \frac{2\pi h(X, Y)}{\lambda}$$

is seriously complicated at $d \ll \lambda$, when the geometric optics approximation is incorrect. The phase 'portrait' undergoes diffractive distortion of both the size and the shape of the subwave structures in the optical inhomogeneity $n(x, y, z)$. Moreover, the overall phase contrast is impaired at $H(x, y) \ll \lambda$. It follows from the above that *a priori* information about the optical model of an object is always helpful for the correct interpretation of phase images containing subwave structures.

Taking into consideration the importance of information about intracellular processes for living cell microscopy, let us consider at greater length the limitations imposed on functional images by the resolving power of an optical system. The notion of a coherent transfer function (or pupil function), with which the criterion for resolution is connected, is correct for amplitude images and only in the paraxial approximation. It is reasonable that the Rayleigh criterion [11] based on the model of two identical point amplitude objects is inapplicable in the general case to functional and phase images. A simple example of an incorrect Rayleigh criterion as applied to functional images, i.e. the detection of object's elements at a distance smaller than $\lambda/2$, is provided by a model of two point sources with nonidentical radiation spectra. In this case, the resolution problem is reduced to the accuracy of determination of source coordinates during measurement of spectral radiation density with the help of two matched filters. The feasibility of superhigh resolution for quasi-point objects with different spectral characteristics has been confirmed in experiment by fluorescence and multiphoton microscopies. Point objects in functional images may differ in a number of characteristics including fluctuation spectra and parameters of motion. This explains why the resolution criteria for functional images are as a rule energy-dependent, and superhigh resolution is achievable at a sufficiently high signal/noise ratio.

Superhigh resolution was also observed in phase images in the course of recording dynamic processes. In this case, the minimum distance between the component spectral density maxima along the scan-line was used as the criterion for resolution.

However, this approach fails to account for both superhigh resolution in phase test-objects [18, 19] and that observed by the differential interference contrast (DIC) technique in amplitude object images [12, 13]. In phase images, the superhigh resolution parameter at a sufficiently high contrast, when

$$\Delta\varphi(X, Y) \cong \pi,$$

amounted to 4–6 [8, 19]. The discrepancy between this approach and the classical theory of optical systems can be removed bearing in mind that the notion of a point coherent transfer function is true only for the paraxial approximation [23, 24].

By the dynamic process in a phase object is meant a uniform sample of OPD values $h(X, Y, t + m\tau)$ in a certain region of coordinates in the image plane X, Y, where $m = 0, 1, 2, \ldots$, τ is the measurement time of one pixel. For definiteness, we shall assume that fluctuations of $h(X, Y, t + m\tau)$ measured by physical methods are in causal relation to a time-dependent refractive index component

$$n(r, t) = n(r) + \delta n(r, t),$$

where $r(x, y, z)$ are the coordinates in the vicinity of the object plane. We shall be further interested in the spatial and temporal characteristics of fluctuating component $\delta n(r, t)$ and their attendant movements. The extraction of useful

biological information $\delta n(r,t)$ from $\Delta\varphi(X,Y,t)$ is equivalent to the solution of the inverse problem, i.e. the determination of the system's dynamic parameters from the scattered wave phases measured in the image plane. It has been mentioned above that the incorrectness of the problem and the ambiguity of its solutions are due to the measurement of a single quantity (OPD) to which contributions are made by many parameters. Therefore, $\delta n(r,t)$ should be formally considered as a functional of many variables.

Physical factors responsible for time-dependent changes of $\delta n(r,t)$ in biological objects are of a great variety. For example, fluctuations $\delta n(r,t)$ in a limited region of coordinates X, Y corresponding to the projection of the cell membrane with the in-built ion channels and enzyme complexes may result from conformational changes in protein molecules, local variations of membrane potential, etc., unrelated to the translational motion of the object as a whole. Such processes are virtually inaccessible to observation by classical microscopic techniques because minor changes of the refractive index have no effect on the intensity of scattered radiation.

Another example of local changes of $\delta n(r,t)$ related to the translational motion is provided by the well-known movements of macromolecules, mitochondria, and other organelles along microtubules, observable by fluorescence microscopy and DIC video microscopy [12, 13, 25].

In phase images, such objects can be formally represented by the function of coordinates (r,t) of the center of a particle with fixed volume V and refractive index

$$\delta n(r,t) = \delta n(r - ut)\,,$$

where u is the projection of average velocity onto the trajectory $r(t)$. If a regular translational motion is accompanied by random or periodic fluctuations, this leads to the appearance of the respective components in the phase fluctuation spectra.

The forthcoming discussion will be confined to considering those forms of motion which can be represented as functions of separable coordinate and time variables:

$$\delta n(r,t) = \sum_m \left\{\delta n_m(r)\exp[j\,\Omega_m\,t]\right\}\,,$$

where $\delta n_m(r)$ denotes functions satisfying boundary conditions, Ω_m stands for frequency eigenvalues, and $m = 1, 2, \ldots$. It is assumed here that local synchronous oscillations occur inside a finite volume V. Therefore, measurements of OPD $h(r,t)$ can yield, in principle, a series of meaningful dynamic parameters of the object, e.g., local frequencies Ω_m of natural oscillations, correlation radii and times, and other characteristics known from the statistical theory of open systems [26].

The measurement results of selected processes will be presented below. For the time being, suffice it to note that the contribution of individual molecules to $\delta n(r,t)$ under real conditions of intracellular microscopy proves to be much smaller than the threshold of sensitivity of interferometers used for the purpose. In the absence of mutual correlation, the spectra are likely to be dominated by stochastic components.

In connection with this, let us consider the dependence of the mean intensity of phase fluctuations on the cross correlation between the movements of object's elements. Let us suppose that in the case of coherent illumination of the object surface from a source of frequency ω, the scattered wave $E_\Sigma(t)$ at a picture site S having coordinates X, Y of the center can be represented by a convolution

$$E(X,Y,t) = \int\!\!\int E(x,y,t)P\left(\frac{X}{M} - x\,,\ \frac{Y}{M} - y\right)\mathrm{d}x\,\mathrm{d}y\,, \quad (2)$$

where $P(X/M - x, Y/M - y)$ is the coherent transfer function, M is the linear magnification factor of the optical system, and

$$E(x,y,t) = \sum_p \left\{a_p(x,y,t)\exp\left(j\left[\omega t + \delta\varphi_p(x,y,t)\right]\right)\right\} \quad (3)$$

is the field of secondary sources from N elements ($1 \leqslant p \leqslant N$) with amplitudes $a_p(t)$ and phases

$$\delta\varphi_p(x,y,t) = \frac{2\pi h(x,y)}{\lambda} = \frac{2\pi}{\lambda}\int n(x,y,z)\,\mathrm{d}z\,.$$

Let these N dynamical objects of identical size be located near the focal plane $z = 0$ inside a layer with boundaries $z = \pm H/2$ (Fig. 2) and represented by a coordinate-independent scalar function of the refractive index

$$n_p(x,y,z,t) = n_p(t)\,.$$

Let us further assume that S is the pixel area in the image plane, the size of which is limited by diffraction on the objective aperture. Then, the integration in formula (2) should be over the area $s = \pi w^2 = S/M^2$ of a circle of radius w, where w is the physical spatial resolution of the microscope. Naturally, an equivalent averaging procedure is also feasible in the image plane X, Y over the circle of area

$$S = \pi W^2\,,$$

where $W/w = M$.

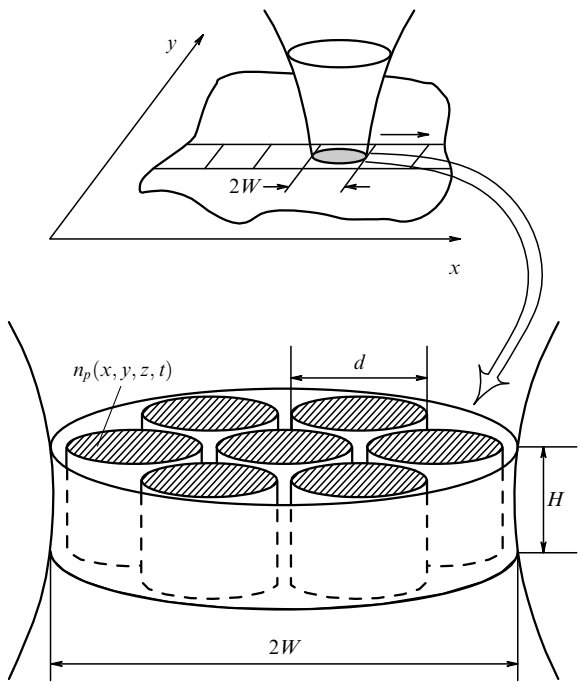

Figure 2. Model of a biological object with N identical elements whose phase fluctuations are partially correlated within one pixel over the area $S = \pi W^2$ of a scattering circle. There is an N-fold rise in the intensity of phase fluctuations of a scattered wave in the case of total spatio – temporal correlation between fluctuations in all elements.

The photodetector in the image plane records the interference field intensity $I_\Sigma(X, Y, t)$ averaged over the pixel area S:

$$I_\Sigma(X, Y, t) = [E_\Sigma + E_r]^2 = I_0 + 2E_0 E_\Sigma(X, Y, t) \cos\left[\varphi(X, Y, t) - \varphi_0(t)\right] = I_0 + I_\sim(X, Y, t)\,,$$

where $E_r(t) = E_0 \exp\left\{j[\omega t + \varphi_0(t)]\right\}$ is the complex reference wave amplitude. From the alternating component $I_\sim(X, Y, t)$ of the photocurrent, it is possible to find (with the aid of a suitable algorithm) the phase $\varphi(X, Y, t)$ of the interference signal averaged over the area S.

Naturally, the contribution of a wave scattered by the object, i.e.

$$\left[E_\Sigma(X, Y, t)\right] \exp\left\{j\varphi(X, Y, t)\right\} = \sum_i \left\{a_i(t) \exp\left(j[\omega t + \delta\varphi_j(t)]\right)\right\},$$

to the phase of the alternating component $I_\sim(X, Y, t)$ of the photocurrent is determined by statistical characteristics $a_p(t)$ and $\delta\varphi_p(t)$.

Let us now find the interdependence of fluctuations $\delta\varphi_p(t)$ and $\delta\varphi(X, Y, t)$ in two limiting cases on the assumption that amplitude fluctuations are absent. Then, for minor fluctuations ($\delta\varphi_p(t) \ll 1$, $\delta\varphi(X, Y, t) \ll 1$), one obtains

$$\delta\varphi(X, Y, t) \cong N^{-1} \sum_p \delta\varphi_p(t)$$

and

$$\left\langle E_\Sigma(X, Y, t)\right\rangle = \sum_p \langle a_p(t)\rangle = N\langle a_p(t)\rangle\,.$$

In the absence of correlation in the phase fluctuations of dynamic objects:

$$\left\langle \delta\varphi_p(t)\, \delta\varphi_r(t+\tau)\right\rangle = 0 \quad (p \neq r)\,,$$

the correlation function of the interference signal phase:

$$K_\Sigma(X, Y, \tau) = \left\langle \delta\varphi(X, Y, t)\, \delta\varphi(X, Y, t+\tau)\right\rangle = N^{-2} \sum_p \sum_r \left\langle \delta\varphi_p(t)\, \delta\varphi_r(t+\tau)\right\rangle = N^{-1} k(\tau) \tag{4}$$

is N times smaller than the correlation function of the phase of an isolated dynamic object: $k(\tau) = \left\langle \delta\varphi_p(t) \times \delta\varphi_p(t+\tau)\right\rangle$.

In the other limiting case of the total phase correlation

$$K_\Sigma(X, Y, \tau) = N^{-2} \sum_p \sum_r \left\langle \delta\varphi_p(t)\, \delta\varphi_r(t+\tau)\right\rangle = k(\tau)\,, \tag{5}$$

where

$$k(\tau) = \left\langle \delta\varphi_p(t)\, \delta\varphi_p(t+\tau)\right\rangle$$

are the equal correlation functions of the phase of the interference signal and the object.

Formulas (4) and (5) are in fair agreement with the well-known conclusion that intensities are summed in uncorrelated processes, and amplitudes in correlated ones.

According to the model in Fig. 2, the correlation between phases $\delta\varphi_p(x, y, t)$ in different elements of the dynamical object ($1 \leqslant p \leqslant N$) is feasible only in the case of correlation between the corresponding fluctuations of the refractive index:

$$\left\langle \delta n_p(t)\, \delta n_r(t+\tau)\right\rangle \neq 0\,.$$

If the fluctuation spectra of individual elements contain dominant frequency components, their spectral density (in the case of correlation)

$$\rho(\Omega) = \frac{1}{2\pi} \int \left\langle n_p(t)\, n_p(t+\tau)\right\rangle \exp(-j\,\Omega\,\tau)\, \mathrm{d}\tau$$

also undergoes an N-fold increase. For small modulation indices $[\delta\varphi_p(x, y, t)] \ll \pi$, the fluctuation spectra of phase and refractive index fluctuations are identical.

It also follows from above that the main contribution to $\delta\varphi(X, Y, t)$ comes from cooperative processes with correlation radii commensurable with or larger than the pixel size. In the case of partial correlation between the processes, their intensities decrease (other things being equal) with increasing number N of independent elements, together with the square of the ratio between the correlation radius R and the resolving power $1/N = (R/W)^2$.

Here is a numerical example to illustrate this inference. Suppose that a local change of the refractive index with amplitude $\delta n(t) = 0.1$ results from conformational transitions in an enzyme (e.g., ATPhase) complex in a region with a linear size $20 \times 10 \times 10$ nm^3 and volume 2×10^{-6} μm^3. Such complexes are arranged in the form of a thin ($H = 20$ nm) layer in the focal plane of the objective of a phase microscope providing a linear resolving power of $W = 0.1$ μm. For the maximum number of enzyme complexes per diffraction spot area $S = \pi W^2$ corresponding to one pixel in the image plane, we find $N \cong 300$. With the intensity of OPD fluctuations of one complex:

$$\sigma_h^2 = \left\langle [H\,\delta n(t)]^2\right\rangle = 2 \text{ nm}^2$$

and in the absence of correlation, the total contribution of all the elements to the OPD is equal to

$$\sum_h \sigma_h^2 = N^{-1}\sigma_h^2 = 6.6 \times 10^{-3} \text{ nm}^2\,.$$

In the opposite case of total correlation between fluctuations of all complexes, the summarized intensity $\sum \sigma_h^2$ is $\sigma_h^2 = 2\,\text{nm}^2$. With the threshold response $h_{\min} = 0.5$ nm, incoherent fluctuations are indistinguishable from the noise, while their coherent summation for a cooperative process gives a high signal to noise ratio $S/N = 4$. If a harmonic component with a coherence time of 10 s is present in correlated fluctuations, its counterpart in the Fourier spectrum is a spectral density $\rho(\Omega) = 20$ nm^2 Hz^{-1}.

3. Laser phase microscope

Airyscan laser phase microscope (Fig. 3) has been developed from the MII-4 LOMO interference microscope [27]. Its optical layout is a modification of the scheme employed in

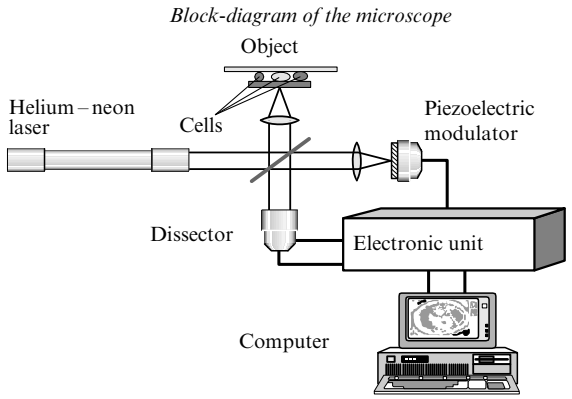

Figure 3. Optical scheme of the Airyscan computerized phase microscope. A cuvette with an object is placed on the stage of the modified Linnik-type microinterferometer and illuminated by a helium – neon laser beam. The linear periodic modulation of the reference wave phase is effected using a mirror with a piezoelectric modulator. A coordinate-sensitive photodetector (dissector image tube) and electronic unit are used for recording the interference signal and its analog-to-digital conversion to the local phase values. Analysis of the phase image and local fluctuations of the optical path difference is performed under computer control.

the Linnik-type microinterferometer. An LG-207A single-mode helium – neon laser ($\lambda = 633$ nm) as the coherent radiation source ensured a high accuracy of phase measurements regardless of the optical path difference between the reference and object beams. The linear periodic modulation of the reference wave phase was achieved using a mirror with a piezoelectric actuator. An LI-620 coordinate-sensitive photodetector (dissector image tube) and electronic unit were used for recording the interference signal and its analog-to-digital conversion to the local phase values.

The dissector image tube was an electrooptical convertor using an external photoelectric effect (without charge accumulation); it was equipped with a photoelectric multiplier and ensured magnetic transfer of the electron flux to the plane of a small orifice diaphragm. The image projected onto the photocathode was scanned by a magnetic field. The spatial resolution depending on the diaphragm orifice diameter was of the order of 200 lines. The size and position of the scanning field were given and monitored by the computer program. The microscope field could be varied within 5 – 50 μm; the maximum image dimension along one coordinate was 1024 pixels. The noise-limited sensitivity was about $h_{\min} = 0.5$ nm. Sampling periodicity and the image input rate were given by a modulation frequency of 1 kHz (or 1 ms per pixel). The object to be examined (cells, organelles) was placed in a 0.3-ml cuvette between a polished silicon substrate and a cover glass. A general view of an Airyscan microscope is shown in Fig. 4. The cuvette with the specimen was placed on the microscope stage. Measurements were made in reflected light.

The software enabled two-dimensional pseudocolor topograms, phase height profiles and the intensity of fluctuations at the arbitrary point of image to be obtained. Also, it made possible recording temporal processes along an arbitrary line in a topogram, subtraction of the trend, and the export of files in ASCII codes.

With this microscope, the compensation method of phase measurement based on a single photocurrent value during the modulation period was realized [22]. The method allowed the moment of compensation to be fixed and the instantaneous

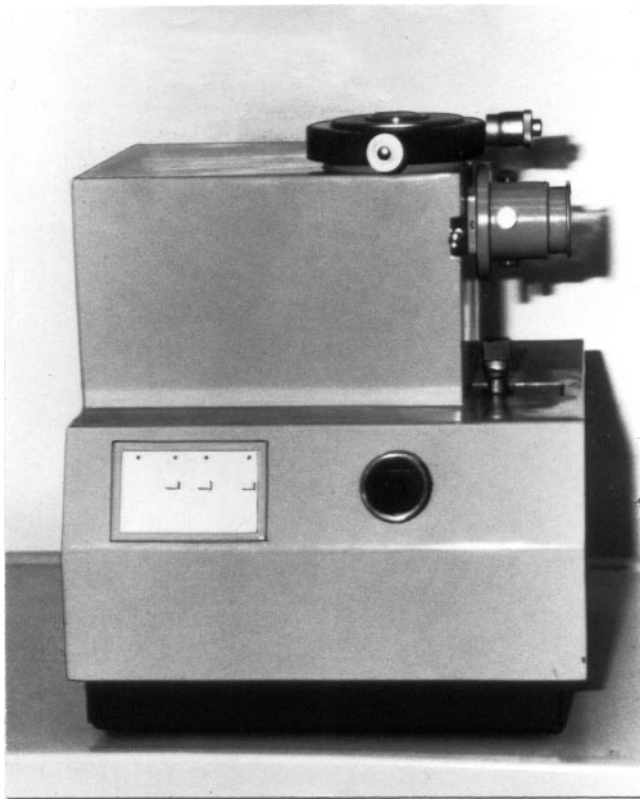

Figure 4. General view of the Airyscan microscope developed on the base of a commercial interference microscope MII-4 LOMO.

phase value to be determined from the length of the normalized time interval. The microscope resolution was tested using standardized semiconducting microstructures and latex spheres of 100 nm in diameter [18, 19]. Measurements by means of dynamic phase microscopy (DPM) were made in the following steps:

(1) *Creation of a phase image*. The photocurrent in the dissector was proportional to the interference field distribution intensity

$$I_\Sigma(X, Y, t) = [E_\Sigma + E_r]^2 = I_0 + 2E_0\, E_\Sigma(X, Y, t) \cos\left[\varphi(X, Y, t) - \varphi_0(t)\right]$$

in each pixel of the image X, Y. The local phase value $\varphi(X, Y, t)$ during the period T of modulation was determined by the time interval method in the electronic unit. The phase image in the form of a matrix of values $\varphi(X, Y, t)$ with the maximum values of raster coordinates M_x, M_y ($0 < X < M_x$, $0 < Y < M_y$) was stored in the computer memory for subsequent processing. The image input time equaled

$$T_\sigma = M_x M_y T\,.$$

The phase image of the object was examined to choose the region of interest from which to extract information about dynamic processes.

(2) *Parameters of temporal sampling*. The DPM technique was applied to obtain information about OPD fluctuations on an interval with the coordinates

$$R_1 = (X_1\,, Y_1) \quad \text{and} \quad R_2 = (X_2, Y_2)\,.$$

The coordinates R_1 and R_2 were fixed on the phase image $\varphi(X, Y)$ of the object. Thereafter, the OPD was measured periodically at an interval of

$$\tau = LT\,,$$

where L is the length of an interval in pixels, by means of p-fold scanning of the interval $R_1 - R_2$. The matrix thus obtained (hereinafter referred to as a track diagram) contained Lp elements, where L is the number of columns, and p is the number of rows equal to the number of repeat scans of the interval $R_1 - R_2$ for time $T_\Sigma = TLp$. The track diagram contained information about processes in each jth pixel of the scan-line ($1 \leqslant j \leqslant L$, $0 < t < T_\Sigma$). The track diagram cross section at a fixed point j gave the 'signal' in the form of a sample of values

$$h_j(t + m\tau) \quad (m = 0, 1, 2, \ldots)\,,$$

from which it was possible to visualize characteristic features of the process. The Fourier transform of the matrix Lp was used to identify the dominant frequency components in the fluctuation spectra $\rho(\Omega, j)$ $(0 < j < L)$ and determine their extent along the scan-line. The spectrum is limited by a frequency

$$F_N = \frac{1}{2\tau} = \frac{1}{2LT}$$

inversely proportional to the scan-line length L; therefore, compromise values of the Nyquist frequency F_N and the scan-line length L were to be found at a given modulation period $T = 1$ ms.

(3) *Correlation and spectral analyses*. Statistical analysis of the processes was performed by the processing of the Lp-matrix. 'Spectral portraits' $\rho(\Omega, j)$ permitted one to determine the spectral density at fixed points j on the scan-line and find the 'profile' $\rho(j)$ of the spectral component $\Omega = \text{const}$. The use of correlators $\langle h_j(t)\, h_i(t + \tau)\rangle$ allowed one to determine the principal statistical characteristics of the processes of interest (OPD fluctuation intensity $\langle h_j(t)^2\rangle$, coherence time, correlation radius, histograms, etc.), compare these functions with the OPD profile $h(X_j)$, and elucidate the relationship between fluctuations and specimen morphology.

DPM also provided limited information about parameters of the particles' translational motion (Fig. 5a). Suppose that a spherical particle with diameter d is in motion in the plane x, y with a constant velocity $\mathbf{v}$ at an angle β to the scan-line S. In the track diagram (Fig. 5b), the 'trace' of the particle that traversed the scan-line for time $\Delta t = d/v_y$ has the form of an ellipse with an inclination α of the major axis and slope

$$\tan\alpha = v_x = \frac{\Delta x - d}{\Delta t}\,.$$

Angle β can be found from the formula

$$\tan\beta = \frac{d}{\Delta x - d}\,.$$

A horizontal section through the middle of the ellipse yields the phase height profile and allows one to determine the diameter of the particle, the profile $h(x)$ of which is depicted in Fig. 5d. If the particle is in nonuniform motion and, besides having a constant component of velocity $\mathbf{v}$, undergoes periodic oscillations $\delta r\cos(\Omega t)$ of coordinates with frequency Ω while the motion of its center is given by

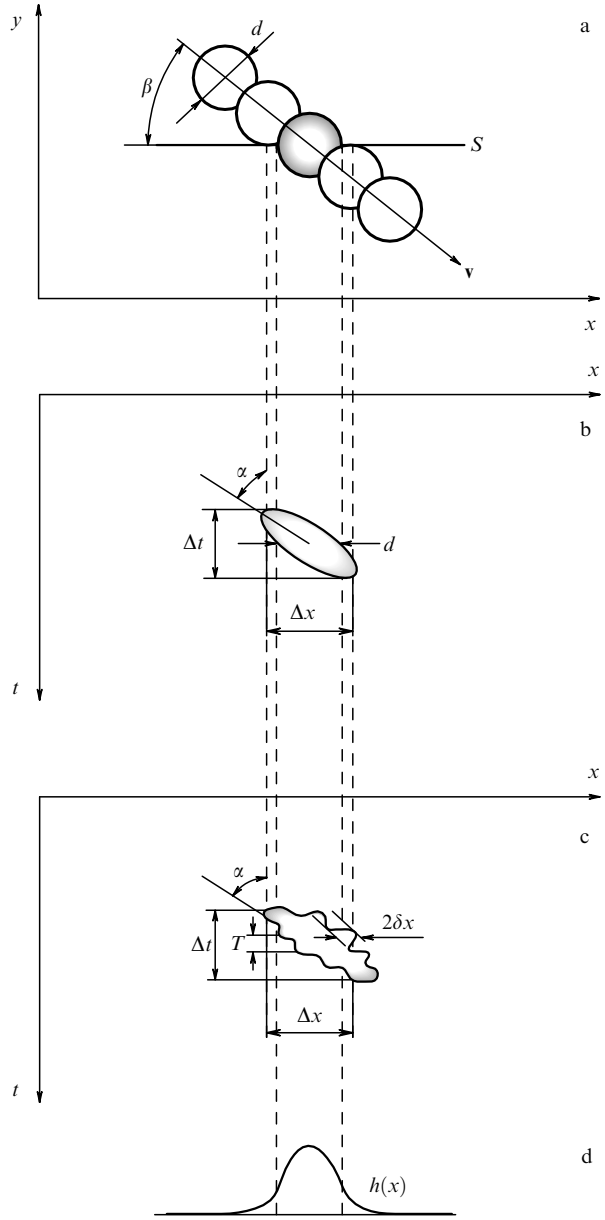

Figure 5. Parameters of the particles' translational motion: (a) a spherical particle with diameter d is in motion in the plane x, y with a constant velocity $\mathbf{v}$ at an angle β to the scan-line S; (b) track diagram shows the 'trace' of the particle that traversed the scan-line for time $\Delta t = d/v_y$ in the form of an ellipse with the inclination α of the major axis and $\tan\alpha = v_x = (\Delta x - d)/\Delta t$; angle β is related to the 'trace' width by the formula $\tan\beta = d/(\Delta x - d)$; (c) in the case of additional periodic oscillations of the particle's coordinates $\mathbf{r}(t) = \mathbf{r}_0 + \mathbf{v}t + \delta\mathbf{r}\cos(\Omega t)$, the 'trace' boundaries also exhibit characteristic oscillations with amplitude $\delta x = \delta r\cos\beta$ and period $T = 2\pi/\Omega$; (d) phase height profile of the particle.

$$r(t) = r_0 + vt + \delta r\cos(\Omega t)\,,$$

its 'trace' boundaries also exhibit characteristic oscillations (Fig. 5c).

4. Informational aspects of living cell phase microscopy

The principal objective of living cell microscopy is to collect new quantitative information about intracellular processes. In order to study cause and effect relations in temporal

processes, measurements should be made in several parts of the object at a time. Because each individual method brings about rather limited information about morphology and local processes, their combination in a single unit always provides additional data owing to simultaneous measurements with different techniques. An example of such units is a combination of DIC and fluorescence microscopes, near-field and conventional far-field microscopes. However, many promising methods of living call microscopy are technically incompatible.

Basic problems for which investigation into the sequence of dynamic processes is crucial for the final result are exemplified by a study of the mitotic cycle phases and mechanisms of programmed cell death (apoptosis). To illustrate, characteristic of the G_1-phase is intense ribosome synthesis in nucleoli [1]. The S-phase is then characterized by active transport of aminoacids across the nuclear membrane and the replication of ribosomes. Centriole replication and spindle formation occur in prophase [1]. Many of these processes exhibit characteristic features of self-organization and spatio–temporal correlation. The central events in apoptosis are the generation of the signal that triggers the expression of suicide genes and the resultant cascade of processes leading to disintegration of intracellular structures. Naturally, well-apparent structural defects are accompanied by even faster conformational modification of macromolecules, changes in ion channel activity, membrane potential, and other characteristics. These variations on the molecular level appear to be responsible for the altered polarizability and local density of the molecules and eventually lead to macroscopic changes of optical parameters.

The hierarchy of intracellular processes is very complicated; thus far, there is no universally accepted approach to its formal description. One of the ways to address the problem is to take advantage of the analogy between the structures of certain types of cellular organelles (membranes, actin-myosin complexes) and that of liquid crystals [28], especially lipid-based ones. In this approximation, a biological object may be viewed as a spatially inhomogeneous dynamic structure whose macroscopic optical properties may be represented by a susceptibility tensor $\chi_{\alpha\beta}(r,t)$ linking the polarization $P_\alpha = \varepsilon_0 \chi_{\alpha\beta} E_\beta$ to the field E (here, $\alpha, \beta = x, y, z$). Signals recorded by optical methods are associated with changes in tensor $\chi_{\alpha\beta}(r,t)$ components and their intensity grows with increasing fluctuation correlation radius. Dynamic light scattering from Williams domains in nematic liquid crystals [28] may serve as an analogue of effects induced in cellular organelles in the course of cooperative processes. We shall proceed from the models used in the physics of liquid crystals and regard the coordinate- and time-dependent refractive index tensor as an adequate order parameter. We do not know the form in which the information controlling spatio–temporal processes in the cell is stored in DNA. It is only conjectured that they are to a considerable degree determinate and safe from the effects of casual factors. We confine ourselves to general considerations and lay aside many questions concerning the physical realizability, consistency, and interpretation of these 'signals'.

The physical grounds of self-organization and conservation of macroscopic order in biological systems have been the subject-matter of many publications starting from the pioneering work of Schrödinger [29]. Papers by Shimizu and Haken [30, 31] devoted to functional relationships between macro- and microsystems have demonstrated the possibility of universally applying the synergetic approach to the description of cooperative processes on the subcellular level. Among the necessary and sufficient conditions of self-organization cited in work [30], there is a key one that reads as follows:

The organelle must have a sufficient number of identical active elements. Their interaction must result in a state described by the order parameter.

It may be supposed that the self-organization conditions discussed by Shimizu and Haken [30] are also fulfilled in certain ensembles of bound enzyme complexes. However, we are unaware of any evidence in support of the existence of coherent states in cellular organelles, associated with order parameter fluctuations at some characteristic frequencies.

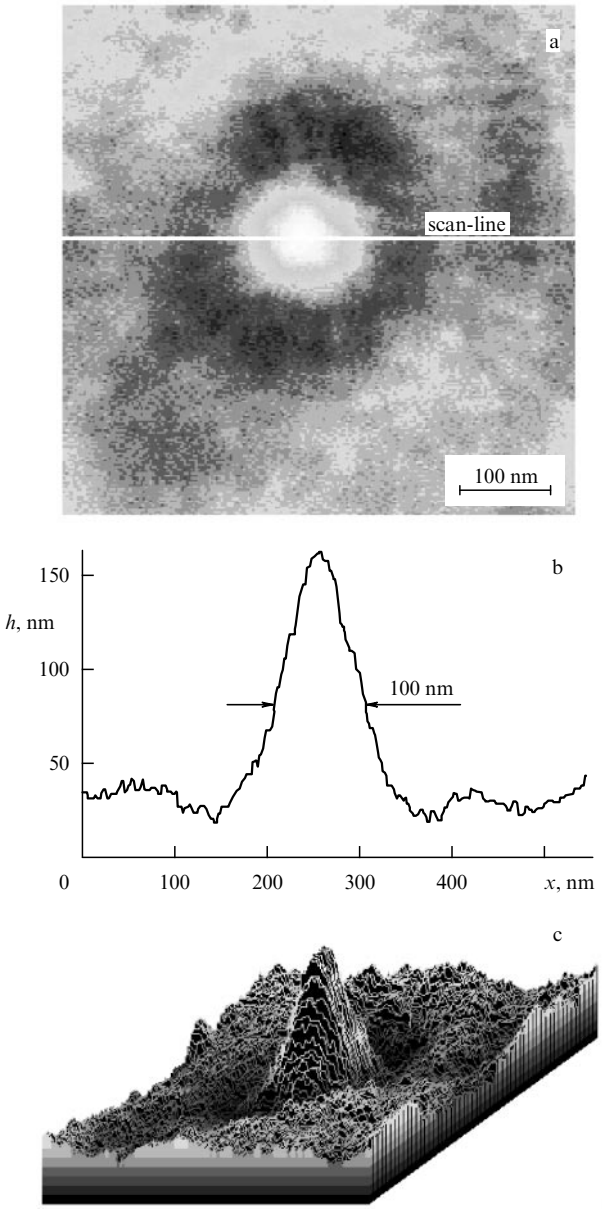

Figure 6. Phase images of a 100-nm latex particle, illustrating the feasibility of superhigh resolution: (a) 2D topogram showing the scan-line; (b) phase height profile along a scan-line; (c) three-dimensional phase image of the particle.

5. Measurement results

Some selected results of measurements reported in this section illustrate the principle of action and potentialities of the microscope described above. Biological specimens in a buffer solution were placed in a cuvette with a polished silicon plate and overlaid by a cover glass. The specimen image was focused visually in coherent light. The working-field size for each objective was certified using a 1200-mm^{-1} diffraction grating.

Figure 6 shows a topogram, phase height profile, and 3D image of a latex particle 100 nm in diameter, which were obtained using a Zeiss objective (100$^{\times}$/0.9). The aqueous latex suspension was layered on the polished substrate and placed on the microscope stage. The suspension dried up, in which case latex particles went visible on the substrate as isolated dots. Focusing to tens of nanometers accuracy was performed based upon the maximum profile contrast in the image scanning regime. Because the resolving power was restricted by diffraction, the profile width and phase height depended on the numerical aperture NA of the objective. For an objective with the numerical aperture $NA = 0.9$ at a wavelength of $\lambda = 633$ nm, the classical Rayleigh resolution was $R_{\mathrm{R}} = 430$ nm. In the case being considered, the superhigh resolution parameter $S_{\mathrm{R}} = R_{\mathrm{R}}/d$ is 4.3, where d is the minimal measured linear size. Measurements using different objectives showed that a noticeable superhigh resolution is achievable only if the aperture is sufficiently large [18]. The maximum profile phase height (OPD) depended on NA and the focusing accuracy. Similar results were obtained for a 100-nm slit in an attested semiconducting structure [18, 19]. The sensitivity $h_{\min} = 0.5$ nm limited by the intrinsic noise was determined from the fluctuation dispersion at a fixed point of the image.

Images of biological objects taken under high magnification showed small-sized structures, however their identification with those visible on an electron microscope was dubious. More reliable interpretation of phase images was achieved when examining relatively large biological objects.

Figure 7 presents a 3D image of a nucleus with the hardly discernible nucleolus at the center of a *Vero* cell in the G_1-phase. The optically denser nucleus is well apparent against the background of the surrounding cytoplasm in the projection

$$h(x, y) = \int n(x, y, z)\,\mathrm{d}z\,.$$

Assuming that the nucleus is a sphere with diameter $d = 7$ μm and the mean phase height difference $\Delta h = 270$ nm as shown in Fig. 7a, the difference between the refractive indices of the nucleus and cytoplasm is estimated as

$$\Delta n \cong \frac{\Delta h}{d} = 0.04\,.$$

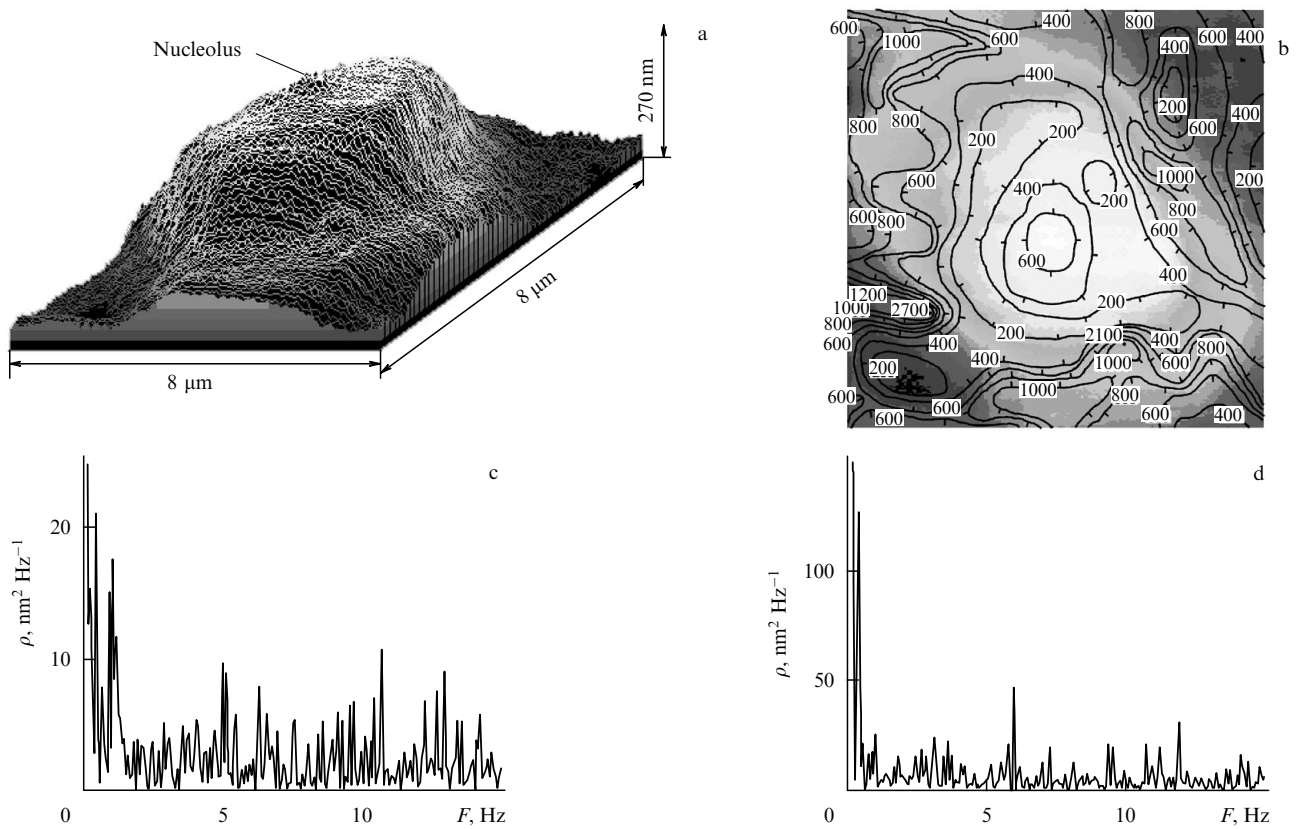

Figure 7. Measurement of fluctuations in a *Vero* karyon in the G_1-phase of the cell cycle: (a) 3D image of the nucleus with the poorly discernible nucleolus at the center (the optically denser nucleus is well apparent in the projection $h(x, y) = \int n(x, y, z)\,\mathrm{d}z$ against the background of the surrounding cytoplasm); (b) nucleus topogram with isolines $I(X, Y)$ of fluctuation intensity in Å^2 (the central peak with $I = 600$ Å^2 is coincident with the nucleolus position); (c) fluctuation spectrum characteristic of this region contains a few contrast components with frequencies $F = 1.5, 5, 6.5$ and 11 Hz; (d) fluctuation spectra at the nucleus periphery (where chromatin condensation near the wall is most pronounced) exhibit contrast components with frequencies $F = 5.9$ and 11.8 Hz.

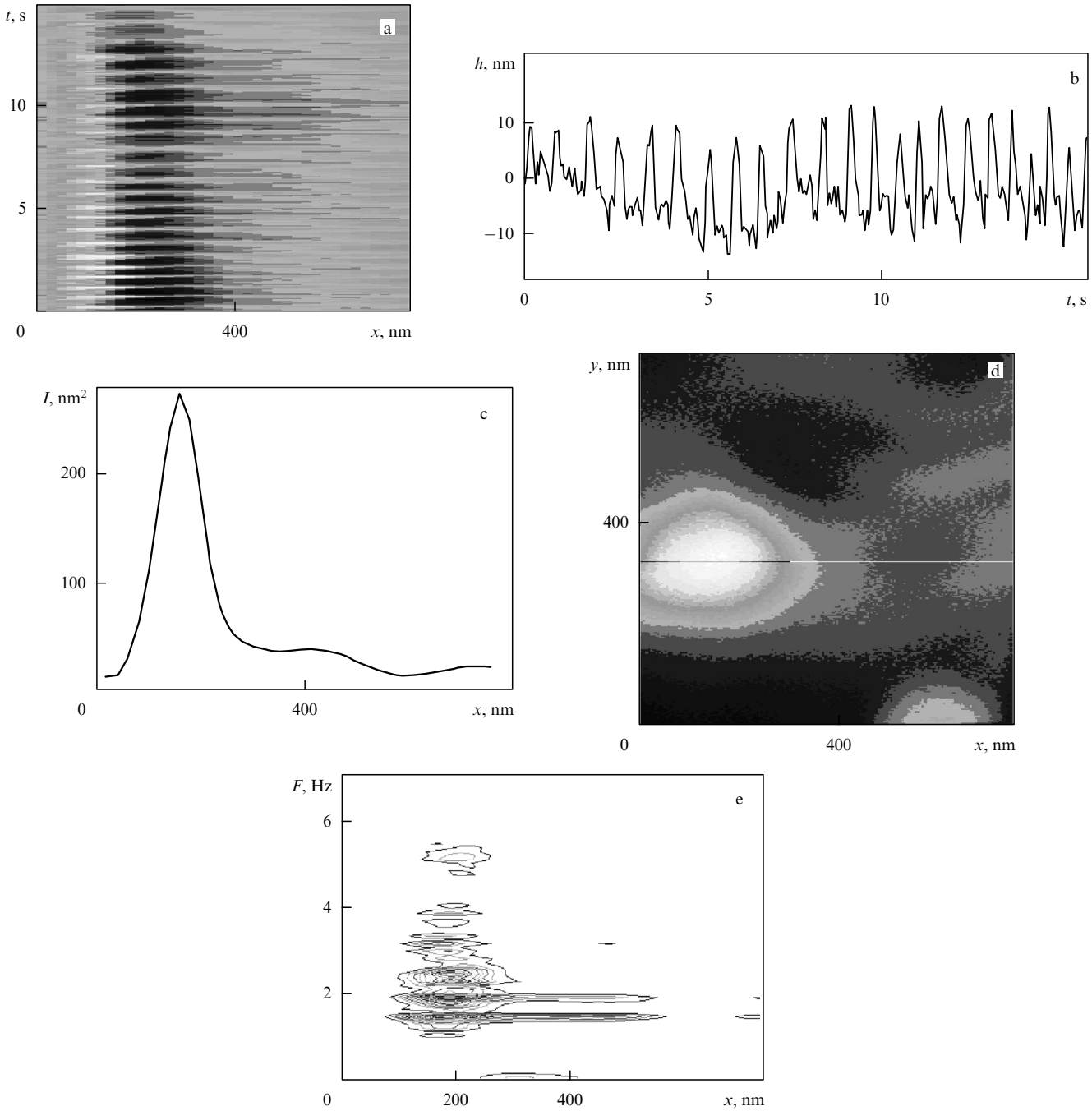

Figure 8. Measurement of beating in bacterium cilia: (a) track diagram of the process with well-apparent horizontal fringes corresponding to periodic changes of OPD on a scan-line of length $\Delta X = 800$ nm for a recording time $T = 15$ s; (b) record made at a fixed point on the scan-line obtained from the vertical section of the track diagram allows one to characterize the peculiarities of cilia movements, the period and amplitude of OPD variations; (c) varying fluctuation intensities along the scan-line points to localization of the process within a region about 150-nm wide, which is distinctly smaller than the size of visually observable bacterium; (d) topogram of a bacterium showing the scan-line; (e) spectral portrait containing additional information about localization of characteristic frequencies. Anharmonic oscillations are apparent only in the vicinity of the maximum. The splitting of the 2 Hz-component is due to variability of the oscillation period throughout the measurement time.

Figure 7b presents a topogram of the nucleus with fluctuation intensity isolines $I(X, Y)$ in Å^2. The peak position at the center, where $I = 600$ Å^2, is coincident with that of the nucleolus. The fluctuation spectrum characteristic of this region (Fig. 7b) contains a few contrast components with frequencies $F = 1.5$, 5, 6.5 and 11 Hz. The nucleolus is known to function as a source of ribosomal subunits. It is therefore supposed that the intensity and frequency of spectral components depend on the rate of biosynthesis. There are a few maxima of up to 2700 Å^2 in intensity at the periphery of the nucleus projection, which may be due to chromatin condensation near the wall. Fluctuation spectra of the peripheral nuclear regions also exhibit contrast components. One such spectrum with components of $F = 5.9$ Hz and $F = 11.8$ Hz is shown in Fig. 7d. The frequency multiplicity appears to reflect the anharmonism of oscillations with a dominant frequency of 5.9 Hz. Intense low-frequency ($F < 0.3$ Hz) components of the spectra are associated with

the slow motion of the nucleus as a whole and the drift of the interferometer. In some cases, the fluctuations were so intense that they were visually discernible in interference images. Figure 8 illustrates such motion and presents the results of measuring beatings in bacterium cilia. Figure 8a shows the track diagram of the process with well-apparent horizontal fringes corresponding to periodic changes of OPD over an interval of $\Delta X = 800$ nm for a recording time $T = 15$ s. The record at a fixed point on the scan-line (Fig. 8b) obtained from the vertical section of the track diagram allowed one to characterize the peculiarities of cilia movements, and the period and amplitude of OPD variations. Figure 8b demonstrates a high ($\cong 20$ nm) OPD amplitude, a varying period of oscillations, and their anharmonicity. It should be recalled that the measured amplitude of OPD changes is much smaller than the real one by virtue of $\Delta n < 1$. A change in fluctuation intensity along the scan-line in Fig. 8c suggests the localization of the process within a region about 150 nm wide, i.e. slightly smaller than the size of visually observable bacteria. The spectral portrait in Fig. 8d contains additional information. Anharmonic oscillations were apparent only in the vicinity of the maximum, whereas harmonic oscillations occur to the right of it. The splitting of the component with frequency 2 Hz is due to period variability as shown in Fig. 8b. It should be noted that the dynamic characteristics of the process are given in absolute units of OPD. This ensures compatibility of measurement results produced with different objects under differing conditions.

Contrast components were also distinguishable in the fluctuation spectra of blood cells, mitochondria, enzyme complexes, and other biological objects.

6. Conclusions

Living cells at different levels of their organization provide an arena for numerous biochemical and biophysical processes accompanied by changes of local macroscopic parameters, which may, in principle, be visualized by optical methods. Variations of the refractive index are most noticeable in phase images belonging to a wide class of functional images. Specific features of functional images of biological objects in coherent light were first considered in the book [32]. The use of coherent light sources was instrumental not only in improving the precision of measurements with phase microscopes but also in implementing a qualitatively new method — dynamic phase microscopy (DPM). This microscopic technique is based on the uniform sample of OPD values along the scan-line in a phase image of the object of interest and subsequent spectral and correlation analyses of the signals. Simple physical reasoning suggests that the main contribution to OPD fluctuations comes from the processes with a large correlation radius which may significantly exceed the transverse size of a single macromolecule in synchronous motion. A simple analysis has demonstrated that the contribution of such cooperative processes under conditions of the spatio – temporal correlation must increase by a factor of N, where N is the number of macromolecules projected onto one pixel. This accounts for the enhanced sensitivity of DPM to spatially correlated and coherent components of fluctuations accompanying cooperative processes.

DNA is a unique material carrier of genetic information that implicitly determines (with restricted determinicity) the sequence of processes at different organizational levels. This genetic information may be conventionally referred to as the 'temporal genome' even though we do not know how the mode in which such information is encoded in the sequence of nucleotide bases enables it to regulate dynamic processes. Naturally, the survival of a biological species would be impossible without reliable mechanisms for the storage, reading, and realization of this information. It may be only conjectured that DNA-controlled processes have a determinate temporal structure which may be revealed, in principle, in the form of optical signals with the aid of noninvasive techniques. Therefore, any attempt is justified to understand the structure of the 'temporal genome', mechanisms controlling dynamic processes, their synchronization and spatio – temporal correlation on the molecular level, using the available optical methods. Of late, there has been increasing interest in single-molecule enzymology [33] which gives hope to identify the real-time sequence of transcription steps for genetic information [34].

The sensitivity of up-to-date fluorescence techniques is sufficient to discover individual macromolecules, but relatively fast dynamic processes in native cells (i.e. containing no fluorescent marks) have until recently remained virtually unamenable to observation on the molecular level. A more realistic approach to this problem is based on the assumption that at least some biological processes involve conformational transitions in macromolecules and may lead to noticeable local macroscopic fluctuations of the refractive index. They can be measured by optical interference methods if the corresponding local values of the OPD are higher than the noise level.

It is far more difficult to identify such optical signals with real processes in a living cell or its organelle. The above examples indicate that contrast spectral components can be identified with a specific intracellular process only in rare cases when the 'structure – function' of the organelle is known. Each cellular element projected onto a given point of the image contributes to dynamic processes. Therefore, several signals from organelles located outside the focal plane may be present in each pixel at a time. Their identification with concrete processes is a difficult task even if the signals are differentiated and their reproducible specific 'phonetic' or structural traits are distinguished. Similar problems of decoding nucleotide sequences of genes have been successfully resolved on the morphological level. In relation to the 'temporal genome', these problems may be conventionally denoted as 'signal – structure – process'. The current knowledge of key biochemical processes and methods for their control provides a solid basis for further progress in this field. Indeed, ATPhase activity is a most promising object for such studies bearing in mind that almost all known biochemical processes are energy-dependent. An ensemble of ATPhase complexes may be regarded as a system of identical active oscillators. Their dynamic interaction gives rise to self-synchronous processes [30] and coherent states characterized by a specific set of eigenfunctions and eigenfrequencies. The correlation radius and coherence time may serve as quantitative characteristics of the degree of cooperativity of the processes that occur in such self-organizing systems.

It is concluded from the above analysis and the results of preliminary investigations that coherent phase microscopy has good prospects for the examination of intracellular processes.

This work was supported by the programme Innovations-Kolleg-27, University of Rostock, Germany and the Russian Federation Ministry of Education. The author thanks

Professor D Weiss and Professor L S Yaguzhinskiĭ for fruitful discussions.

References

1. Bruce A B et al. *Molecular Biology of the Cell* 3rd ed. (New York: Garland Publ., 1994)
2. Straub M, Hell S W *Appl. Phys. Lett.* **73** 1769 (1998)
3. Schrader M, Hell S W *J. Appl. Phys.* **84** 4033 (1998); Hell S W, Nagorni M *Opt. Lett.* **23** 1526 (1998)
4. Farkas D L et al. *Comput. Med. Imag. Graph.* **22** 89 (1998)
5. Mehta A D et al. *Science* **283** 1689 (1999)
6. Noji H et al. *Nature* **386** 299 (1997)
7. De Beer E L et al. *Cell Motil.* **38** 341 (1997)
8. Tuvia S et al. *Proc. Natl. Acad. Sci.* **94** 5045 (1997)
9. Farkas D L et al. *Annu. Rev. Physiol.* **55** 785 (1993)
10. Wachman E S, Nju W, Farkas D L *Biophys. J.* **73** 1215 (1997)
11. Born M, Wolf E *Principles of Optics* (Oxford: Pergamon Press, 1965) [Translated into Russian (Moscow: Nauka, 1970) p. 87]
12. Weiss D G et al., in *Light Microscopy in Biology — A Practical Approach* (Ed. A J Lacey) (Oxford: Oxford, University Press, 1999) p. 73
13. Innoue S, Spring K R *Video Microscopy: The Fundamentals* 2nd ed. (New York: Plenum Press, 1997)
14. Schneider B et al., in *Fluorescence Microscopy and Fluorescent Probes* Vol. 2 (Ed. J Slavic) (New York: Plenum Press, 1998) p. 63
15. Edelmann P et al. *Optik* **110** 194 (1999)
16. Tychinsky V et al. *Proc. SPIE* **1647** 96 (1992)
17. Tychinsky V et al. *Proc. SPIE* **2100** 129 (1993)
18. Tychinsky V P *Kvantovaya Elektron.* **24** (8) 754 (1997)
19. Tychinsky V P *Pis'ma Zh. Tekh. Fiz.* **17** (22) 80 (1991)
20. Schmit J, Creath K *Proc. SPIE* **2544** 102 (1995)
21. Creath K *Proc. SPIE* **1319** 318 (1990)
22. Tychinsky V P, Zakharov V P, Snezhko Yu A *Kvantovaya Elektron.* **6** 114 (1996)
23. Solimeno S, Crosignani B, Di Porto P *Guiding, Diffraction, and Confinement of Optical Radiation* (New York: Acad.Press, 1986) [Translated into Russian (Moscow: Mir, 1989)]
24. Tychinskiĭ V P *Usp. Fiz. Nauk* **166** 1219 (1996) [*Phys. Usp.* **39** 1157 (1996)]
25. Weiss D G, Seitz-Tutter D, Langford G M *J. Cell Sci.* **S14** 157 (1991)
26. Klimontovich Yu L *Statisticheskaya Teoriya Otkrytykh Sistem* (Statistical Theory of Open Systems) (Moscow: Yanus, 1995) [Translated into English (Dordrecht: Kluwer Acad. Publ., 1995)]
27. Tychinsky V P et al. *Opt. Commun.* **74** 37 (1989)
28. De Gennes P G *The Physics of Liquid Crystals* (Oxford: Clarendon Press, 1974) [Translated into Russian (Moscow: Mir, 1977)]
29. Schrödinger E *What is Life?* (Cambridge: The University Press, 1944)
30. Shimizu H, Haken H *J. Theor. Biol.* **104** 261 (1983)
31. Shimizu H *Adv. Biophys.* **13** 195 (1979)
32. Ivanitskiĭ G R, Kuninskiĭ A S *Issledovanie Mikrostruktury Ob'ektov Metodami Kogerentnoĭ Optiki* 2nd ed. (Microstructural Studies by Coherent Optics Techniques) (Moscow: Energiya, 1981)
33. Xie S X, Lu H P *J. Biol. Chem.* **274** 15967 (1999)
34. Harada Y et al. *Nature* **409** 113 (2001)